Overlooked Activation Role of Sulfite in Accelerating Hydrated Electron Treatment of Perfluorosulfonates

Zhiwen Jiang, Sergey Denisov, Daniel Adjei, Mehran Mostafavi, Jun Ma

Environmental Science & Technology

pubs.acs.org/est

Article

Overlooked Activation Role of Sulfite in Accelerating Hydrated Electron Treatment of Perfluorosulfonates

Zhiwen Jiang, Sergey Denisov, Daniel Adjei, Mehran Mostafavi,* and Jun Ma*

Cite This: https://doi.org/10.1021/acs.est.4c01444

Read Online

ACCESS | Metrics & More | Article Recommendations | Supporting Information

ABSTRACT: Photoexcitation of sulfite (SO_3^{2-}) is often used to generate hydrated electrons (e_{aq}^-) in processes to degrade perfluoroalkyl and polyfluoroalkyl substances (PFASs). Conventional consensus discourages the utilization of SO_3^{2-} concentrations exceeding 10 mM for effective defluorination. This has hindered our understanding of SO_3^{2-} chemistry beyond its electron photogeneration properties. In contrast, the radiation-chemical study presented here, directly producing e_{aq}^- through water radiolysis, suggests that SO_3^{2-} plays a previously overlooked activation role in the defluorination. Quantitative ^{60}Co gamma irradiation experiments indicate that the increased SO_3^{2-} concentration from 0.1 to 1 M enhances the defluorination rate by a remarkable 15-fold, especially for short-chain perfluoroalkyl sulfonate (PFSA). Furthermore, during the treatment of long-chain PFSA ($C_8F_{17}-SO_3^-$) with a higher concentration of SO_3^{2-}, the intermediates of $C_8H_{17}-SO_3^-$ and $C_3F_7-COO^-$ were observed, which are absent without SO_3^{2-}. These observations highlight that a higher concentration of SO_3^{2-} facilitates both reaction pathways: chain shortening and H/F exchange. Pulse radiolysis measurements show that elevated SO_3^{2-} concentrations accelerate the bimolecular reaction between e_{aq}^- and PFSA by 2 orders of magnitude. ^{19}F NMR measurements and theoretical simulations reveal the noncovalent interactions between SO_3^{2-} and F atoms, which exceptionally reduce the C−F bond dissociation energy by nearly 40%. As a result, our study offers a more effective strategy for degrading highly persistent PFSA contaminants.

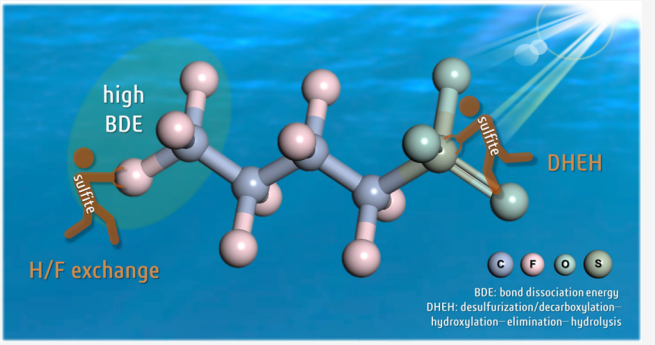

KEYWORDS: *pulse radiolysis, transient kinetic, perfluoroalkyl sulfonate, defluorination, hydrated electron reduction, SO_3^{2-} effect*

INTRODUCTION

Hydrated electron (e_{aq}^-)-based advanced reduction processes (e_{aq}^--ARP) have been notable contenders to address the challenges of the "forever pollutant" per- and polyfluoroalkyl substances (PFASs) degradation.[1−3] Generally, the highly reactive e_{aq}^- is produced via water radiolysis or photoexcitation with sensitizers like sulfite (SO_3^{2-}), iodine (I^-), and nitrilotriacetic acid.[4−6] SO_3^{2-} has garnered significant attention due to its moderate quantum yield (0.11−0.17 mol/einstein) ($SO_3^{2-} + h\nu \rightarrow SO_3^{\cdot-} + e^-$) and inert byproducts to prevent undesired reactions during photolysis.[7−9] Consequently, extensive studies have chosen SO_3^{2-} as the cornerstone for optimizing defluorination performance. These optimization strategies include pH adjustment,[10] iodide addition,[11] and the integration with oxidants ($^{\cdot}OH$).[7,8] For instance, Liu and co-workers[10] reported that at pH 12, e_{aq}^- effectively cleaves multiple robust C−F bonds that remain unaltered at pH 9.5. The high pH condition determines the speciation of dissolved carbonate to prevent e_{aq}^- quenching. In this case, the decarboxylation pathway is notably favored toward extensive defluorination and the reduction of SO_3^{2-} consumption. Besides, the addition of iodide and other halogens in the UV/SO_3^{2-} system has demonstrated the capacity to increase e_{aq}^- concentration and accelerate PFAS degradation rates.[11,12] However, our previous research has unveiled the chain length dependence on the reaction rate of PFSA with e_{aq}^-.[13] The specific rate constant for the reaction of perfluorobutanesulfonate (PFBS) with e_{aq}^- is less than 10^6 M^{-1} s^{-1} under the pH = 10 condition. This implies that e_{aq}^--ARP is ineffective against short-chain PFAS.[13,14] Therefore, searching for a new strategy to enhance the reactivity of short-chain PFAS with e_{aq}^- becomes highly desirable.[15,16]

The significance of SO_3^{2-} beyond electron generation has rarely been rarely appreciated. The limited understanding of SO_3^{2-} has posed discrepancies in current PFAS treatment based on the UV/SO_3^{2-} system with different SO_3^{2-} concentrations. Tang and co-workers[9] suggested that the

Received: February 7, 2024
Revised: April 19, 2024
Accepted: May 7, 2024

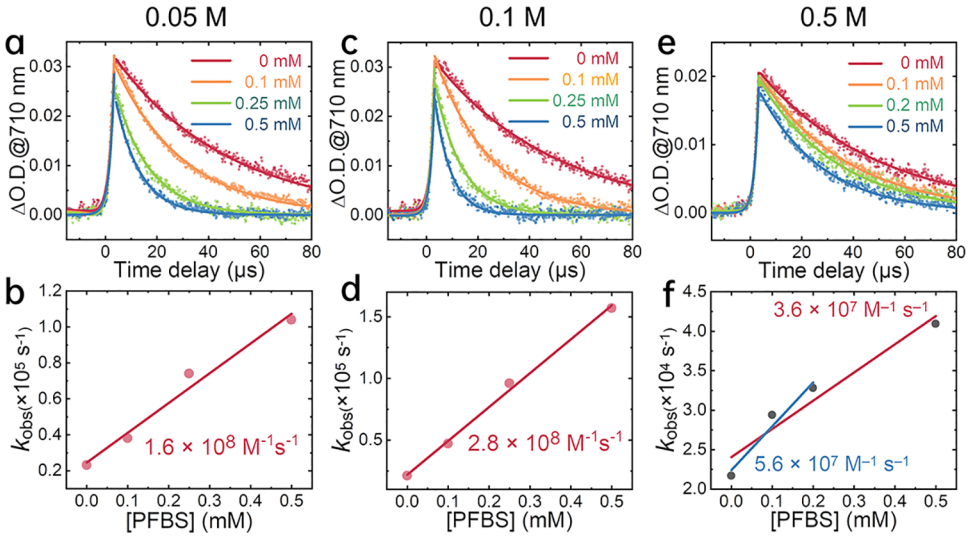

Figure 1. Pulse radiolysis measurements on an Ar-saturated solution containing three concentrations of SO_3^{2-}: the decay at 710 nm (a) and apparent e_{aq}^- decay rate (b) as a function of PFBS concentration under 0.05 M SO_3^{2-}; the decay at 710 nm (c) and apparent e_{aq}^- decay rate (d) as a function of PFBS concentration under 0.1 M SO_3^{2-}; and the decay at 710 nm (e) and apparent e_{aq}^- decay rate (f) as a function of PFBS concentration under 0.5 M SO_3^{2-}.

increasing SO_3^{2-} concentration (ranging from 0.5 to 20.0 mM) led to a roughly linearly increase in the generation rate of e_{aq}^-. However, Liu et al.[11] argued that further increasing the concentration of SO_3^{2-} (e.g., 20 mM) did not improve performance. It is postulated that a high concentration of SO_3^{2-} might trigger a competing side quenching reaction.[17−20] Existing paradigms have constrained photolysis studies to SO_3^{2-} concentrations below 20 mM. Such a low concentration precludes the investigation of potentially beneficial effects of SO_3^{2-} in PFAS treatment. For example, a high SO_3^{2-} concentration may primarily induce the self-assembly of micelles. The rapid e_{aq}^- transfer in the micelles may enhance PFAS defluorination.[21] Moreover, the oxidation process involved in PFAS treatment caused by $SO_3^{\cdot-}$ radicals from photolysis on SO_3^{2-} remains controversial. The comprehensive exploration of the interaction between SO_3^{2-} and PFAS has also been notably underemphasized.

In addition to photolysis, the radiolysis of aqueous SO_3^{2-} solutions using commercial radiation sources such as ^{60}Co γ-rays and electron beams has been a promising advanced reducing process to tackle PFSA pollution.[22−24] Over the past decades, the utilization of safe, energy-saving, and controllable irradiation setups has demonstrated their capabilities in pilot-scale wastewater treatment.[24,25] The fundamental principle involves the ionization and excitation of water by radiation, leading to the generation of abundant short-lived species such as oxidizing $^{\cdot}$OH radicals and e_{aq}^-. These short-lived species exhibit high reactivity toward specific organic pollutants.[25,26] In the radiolytic method, SO_3^{2-} scavenge $^{\cdot}$OH radicals to form $SO_3^{\cdot-}$ radicals. It was known that radiolysis of SO_3^{2-} aqueous solution creates enhanced reducing conditions that likely increase the defluorination efficiency.[26,27] Moreover, the generation of e_{aq}^- through water radiolysis remains independent of photosensitizers. These advantages enable us to investigate the overlooked SO_3^{2-} chemistry and develop more effective approaches for short-chain PFAS degradation.[28] More importantly, the elementary reactions of PFAS with e_{aq}^- or $SO_3^{\cdot-}$ radicals can be studied by pulse radiolysis, involving transient kinetics and intermediate identification by time-resolved spectroscopy. Here, we measured the bimolecular rate constant between e_{aq}^- and PFSA under various SO_3^{2-} concentrations. Combined with product analysis via steady-state ^{60}Co irradiation, we find that the presence of SO_3^{2-} encompasses the interaction with F atoms to facilitate C−F bond cleavage and activates C−S bonds for a more readily desulfonation pathway simultaneously. The bond interactions are supported by NMR observations and theoretical calculations, which culminate in a profound defluorination process.

MATERIALS AND METHODS

The experiments and analysis methods are more detailed in the Supporting Information (SI). Briefly, potassium heptadecafluoro-1-octanesulfonate ($C_8F_{17}SO_3K$, PFOS) and potassium perfluorobutanesulfonate ($C_4F_9SO_3K$, PFBS) were purchased from Sigma-Aldrich and were used as received. Pulse radiolysis experiments were carried out employing the picosecond laser-triggered electron accelerator, ELYSE, coupled with a time-resolved absorption spectrophotometric detection system (290−720 nm).[29,30] More details for pulse radiolysis measurements can be found in the recent work.[17] The steady-state experiments were conducted at a ^{60}Co gamma source (5.35 × 10^{13} Bq, located in the Université Paris-Saclay) at a dose rate of 2.25 kGy/h at ambient conditions with Ar-saturated solutions. The sample solutions were prepared in ultrapure water (18.2 MΩ cm), and the pH was adjusted with a NaOH solution without buffer. The concentration of fluoride ion (F^-) released from PFSA was determined by an ion-selective electrode (ISE), which is used to calculate the defluorination number. ^{19}F (376 MHz) and ^{1}H (400 MHz) NMR spectra were recorded on a BRUKER AVANCE III NMR spectrometer equipped with a QXO (Quattro Resonance X Observe) probe, using D_2O as the solvent. Potassium fluoride (KF) was employed as a reference to calibrate the chemical shift. Product analysis was conducted by liquid chromatography−high-resolution mass spectrometry (LC−HRMS). DLS measurements were performed on a Zetasizer Lab instrument (Malvern Instruments) with a He−Ne laser of λ = 633 nm. The C−F

https://doi.org/10.1021/acs.est.4c01444
Environ. Sci. Technol. XXXX, XXX, XXX−XXX

bond dissociation energy (BDE) for all PFASs examined in this study was calculated by using the GAUSSIAN 16 program. All the geometries of molecular, intermediate, and transition states were fully optimized using the Grimme empirical dispersion corrected B3LYP-D3/6-311+G(2d,2p) hybrid functional energies. The solvation model based on density theory (SMD) was applied to simulate the aqueous environment implicitly. The details of experimental methods and theoretical calculations can be found in the Supporting Information (SI).

RESULTS AND DISCUSSION

e_{aq}^- Reaction with PFBS in SO_3^{2-} Solution. First, we conducted the reaction of PFSA with e_{aq}^- under the alkaline condition (pH = 12) in the absence of SO_3^{2-}. The transient kinetics recorded at 710 nm, corresponding to the maximum of the absorption band of e_{aq}^-, exhibited no significant change in the e_{aq}^- decay in the presence of PFBS. The pseudo-first-order rate constant was estimated to be less than 10^6 M^{-1} s^{-1}, consistent with previous findings.[13,14,31] This low rate constant indicated that PFBS remained chemically inert to e_{aq}^- without adding SO_3^{2-} (Figure S1).

In stark contrast, Figure 1a–f presents compelling evidence of accelerated e_{aq}^- decay in solutions containing SO_3^{2-} ranging from 0.05 to 0.5 M. e_{aq}^- decayed faster with rising PFBS concentration. The second-order rate constants were determined to be 1.6×10^8 and 2.8×10^8 M^{-1} s^{-1} in the presence of 0.05 and 0.1 M SO_3^{2-}, respectively. These rates represented an enhancement of more than 2 orders of magnitude compared to that in the absence of SO_3^{2-} (Figure 1b–d). Nevertheless, a noticeable deceleration in e_{aq}^- decay occurred when the SO_3^{2-} concentration exceeded 0.5 M (Figure 1e,f). In this case, the apparent rate of decay deviated from a linear relationship with the PFBS concentration and decreased to $3.6–5.6 \times 10^7$ M^{-1} s^{-1} (Figure 1e,f). The decrease in rate constants is likely attributed to the aggregation or micellization process of PFBS. This is often observed in higher ionic strength solutions for surfactant systems.[32,33] Based on the surfactant characteristics of PFBS, it is presumed that the higher SO_3^{2-} concentration diminished the electrostatic repulsion between negatively charged headgroups of PFBS. The reduced repulsion fostered aggregation and micelle formation. The aggregation and micellization process ultimately decreased notably the reactivity of PFBS with e_{aq}^-.

Water radiolysis generates reducing e_{aq}^- and oxidizing $^{\cdot}OH$ radicals. SO_3^{2-} also reacts with $^{\cdot}OH$ radicals to form $SO_3^{\cdot-}$ radical, a typical reactive oxidant employed for degrading organic pollutants.[34,35] To explore the possible reaction of PFBS with the $SO_3^{\cdot-}$ radical, we conducted pulse radiolysis experiments in an N_2O-saturated solution (Figure 2). Under this condition, e_{aq}^- is initially converted to $^{\cdot}OH$ radical (Figure S2) ($N_2O + e_{aq}^- \rightarrow O^{\cdot-} + N_2$ $k_2 = 6.0 \times 10^9$ M^{-1} s^{-1}; $O^{\cdot-} + H_2O \rightarrow {}^{\cdot}OH + OH^-$ $k_3 = 9.3 \times 10^7$ M^{-1} s^{-1}). Subsequently, $SO_3^{\cdot-}$ radicals are generated as the sole reactive species in the solution ($^{\cdot}OH + SO_3^{2-} \rightarrow H_2O + SO_3^{\cdot-}$ $k_4 = 5.1 \times 10^9$ M^{-1} s^{-1}). As illustrated in Figure 2a, when e_{aq}^- was completely quenched, the transient absorption at 10 μs displayed characteristic spectra of $SO_3^{\cdot-}$ radicals in the UV regions. The kinetics at 310 nm revealed the identical decay of $SO_3^{\cdot-}$ radicals in the presence or absence of PFBS with a half-time of 40 μs (Figure 2b). The decay of $SO_3^{\cdot-}$ radicals did not exhibit any dependence on the PFBS concentration. Based on the transient data excluding any reactivity between $SO_3^{\cdot-}$ and PFBS, we concluded that SO_3^{2-} instead of $SO_3^{\cdot-}$ radicals played an active role in accelerating the bimolecular reaction between e_{aq}^- and PFBS.

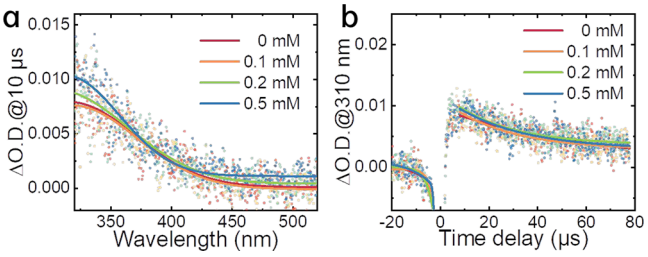

Figure 2. Pulse radiolysis measurements on N_2O-saturated 0.2 M SO_3^{2-} solution in the presence of different concentrations of PFBS. (a) Transient absorption spectrum at 10 μs corresponding to $SO_3^{\cdot-}$ radicals. (b) Transient kinetic traces of $SO_3^{\cdot-}$ radicals at 310 nm within 80 μs.

Interactions between SO_3^{2-} and PFBS. Subsequently, we performed ^{19}F nuclear magnetic resonance (NMR) spectroscopy in a 0.5 mM PFBS solution to elucidate the interaction between PFBS and SO_3^{2-}. KF was employed to calibrate the chemical shift. In our samples, we observed four distinct signals within the chemical shift range from −79.9 to −125.0 ppm. These signals were assigned to distinct F positions in the PFBS molecular framework (Figure 3a).[36,37] Significantly, the signals consistently exhibited a downfield shift when 0.1 M SO_3^{2-} is present (Figure 3b–e). These shifts signified a reduced electron density around F atoms, which could be attributed to the interaction from SO_3^{2}.[38−40] Importantly, these observations cannot be ascribed to the aggregation and micellization because the processes typically induce an upfield shift in the F signal, as previously reported.[39,41] The downfield shifts strongly suggested that the formation of interactions predominated the influence of SO_3^{2-} on PFBS rather than micellization. Furthermore, when SO_3^{2-} underwent protonation under pH 6, no shift in the F signals occurred since these protonated ions were unable to form interactions with the F atoms. This contrast between SO_3^{2-} and its protonated counterpart suggests that this interaction is chiefly driven by the lone pair of electrons residing on the sulfur atom in SO_3^{2-}, leading to the unexpected activation of C−F bonds.

Along with the increase in the SO_3^{2-} concentration up to 0.5 M, all observed signals experienced more pronounced shifts toward the downfield region. Specifically, the chemical shift of F_δ exhibited the most substantial change, amounting to a remarkable 0.062 ppm shift, while those of F_α and F_γ both shifted by 0.040 ppm toward the downfield. However, the chemical shift of F_β showed only a slightly smaller change of 0.030 ppm. The magnitude of the observed chemical alterations in NMR follows a sequence of $F_\delta > F_\alpha \approx F_\gamma > F_\beta$. Intriguingly, this tendency corresponds closely with the change of the theoretically calculated C−F bond dissociation energies (BDEs).[28,42] The C−F bond BDEs of the terminal $-CF_3$ (118.8 kcal mol^{-1}) are significantly higher than those of the C−F bonds in the middle $-CF_2-$ moieties (106.5−109.2 kcal mol^{-1}). The significant shift implied that SO_3^{2-} effectively formed interactions with the more recalcitrant F atoms and activated the corresponding C−F bonds that are conventionally challenging to break. This mechanism may play a pivotal role in substantially enhancing the defluorination rate.

The significance of SO_3^{2-} in the acceleration of defluorination was further illustrated by density functional theory (DFT)

https://doi.org/10.1021/acs.est.4c01444
Environ. Sci. Technol. XXXX, XXX, XXX−XXX

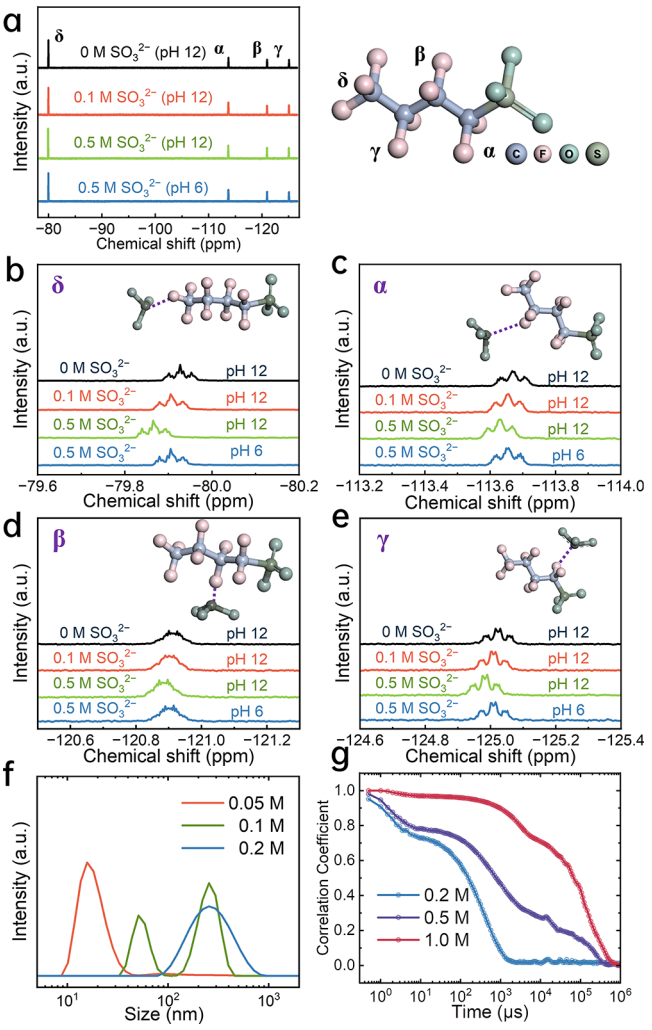

Figure 3. ^{19}F NMR spectra of PFBS (0.5 mM) in the presence of different concentrations of SO_3^{2-} and PFBS molecule model (a), and corresponding spectra for F_δ region (b), F_α region (c), F_β region (d), and F_γ region (e). Inset: The optimized structure of PFBS and the SO_3^{2-} complex. DLS size distribution (f) and correlation data (g) of PFBS in the presence of different SO_3^{2-} concentrations.

calculations. As expected, the geometries and electron distribution of the optimized structures of PFBS with SO_3^{2-} suggested weakly bound, noncovalent complexes between F atoms and SO_3^{2-}. When SO_3^{2-} was approaching the PFBS molecule, the spatial configuration of SO_3^{2-} was converted from a triangular conical to a planar structure (Figure 3b−e). Meantime, compared with single PFBS, the LUMO of the complex was mainly located on the SO_3^{2-} and its interacting F atoms with a clear sigma antibonding nature (Figure S3). Once an external electron is attached to PFBS, SO_3^{2-} would "lead" itself to localize in the F atoms and induce C−F cleavage. As summarized in Table 1, the bond dissociation energies (BDEs) of C−F bonds in PFBS molecules were calculated through both homolytic and heterolytic dissociation. According to previous studies,[10,14] the primary C−F bond (F_δ, 117.8 kcal mol^{-1}) presented higher BDEs than all secondary C−F bonds (F_α, F_β, F_γ, 107.0−109.4 kcal mol^{-1}). F_β had lower BDEs in all C−F BDEs, 107.0 kcal mol^{-1}. In our cases, SO_3^{2-} sharply decreased the BDE of the C−F on the adjacent F atoms for homolytic reactions. Specifically, the BDE of the primary C−F bond (F_δ) dropped by nearly 60% to 47.8 kcal mol^{-1}, and other BDEs declined to around 36.2−39.1 kcal mol^{-1}.

Table 1. Calculated C−F BDEs (kcal mol^{-1}) of PFBS with the B3LYP-D3(BJ)/6-31G* Level of Theory

	homolytic reaction			heterolytic reaction		
C−F bond type	BDEs without SO_3^{2-}	BDEs with SO_3^{2-}	difference	BDEs without SO_3^{2-}	BDEs with SO_3^{2-}	difference
α	109.4	39.1	70.3	99.3	98.9	0.4
β	107.0	36.2	70.8	97.3	96.4	0.9
γ	108.9	38.7	70.2	102.2	101.7	0.5
δ	117.8	47.8	70	95.7	95.4	0.3

We also simulated the potential transition state to investigate the interaction between PFAS and sulfite (Figure S4). The geometry of the transition state for PFAS in the presence of sulfite showed significant stretched C−F bonds when compared to the pristine PFAS configuration. Specifically, the C−F bond length in the terminal $-CF_3$ group expanded from 1.35 to 2.13 Å, while the corresponding bond length in the middle $-CF_2-$ unit enlarged from 1.54 to 2.14 Å. The stretched C−F bonds demonstrated the interaction between the sulfite's oxygen atom and F atoms within the PFAS molecule (Figure S4a,b), highlighting the chemical reactivity and potential transformation pathways of PFAS in sulfite-rich environments. It is noted that the corresponding energy of the terminal $-CF_3$ transition state (38.6 kcal mol^{-1}) was found to be 1.5 times higher than that of the middle $-CF_2-$ moieties (25.3 kcal mol^{-1}). However, in the presence of explicit water molecules, we did not find similar transition states of PFAS with sulfite (Figure S4c). The role of explicit water molecules is indispensable during defluorination by hydrated electrons. We speculated that sulfite dominated the interaction with F atoms and explicit water molecules might interact with them by more complex structures. To the best of our knowledge, such a significant reduction in BDEs by noncovalent interactions has never been reported. The distinctive reduction in BDEs clearly reveals that the introduction of SO_3^{2-} lowered reaction energy barriers of e_{aq}^- defluorination.

To investigate PFBS aggregation at higher SO_3^{2-} concentrations, dynamic light scattering (DLS) measurements were carried out. The peak shifted from 15.6 to 255 nm (Figure 3f) as the SO_3^{2-} concentration increased from 0.05 to 0.2 M.[43] This shift indicated a notable enlargement of the size distribution of PFBS aggregates. We performed the DLS measurements on 0.5 mM PFBS solutions without sulfite as a control experiment (Figure S5). After 1 h, the peak of the size distribution remains almost the same. Furthermore, considering that the concentration of PFBS in our experiments (0.5 mM) was much lower than its CMC (22 mM), it can be inferred that the presence of alcohol had a negligible effect on the aggregation behavior of PFBS. These control experiments underscored the minimal impact of alcohol on the system. Furthermore, as the concentration exceeded 0.2 M, the time correlation function curves systematically shifted toward longer time scales (Figure 3g). These findings pointed out that the high concentration of SO_3^{2-} induced the formation of larger PFBS aggregates or micelles and thus slowed the dynamics of reactants.[44,45] To conclude, the introduction of SO_3^{2-} induced a set of interrelated effects on the PFBS molecular configuration. On the one hand, SO_3^{2-} interacted with F atoms and played a catalytic role in activating C−F bonds for

https://doi.org/10.1021/acs.est.4c01444
Environ. Sci. Technol. XXXX, XXX, XXX−XXX

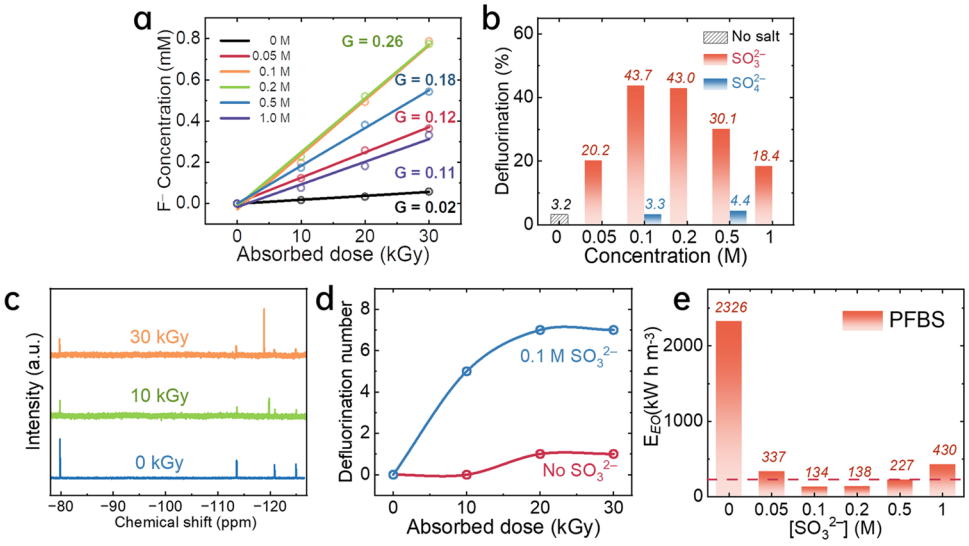

Figure 4. (a) Radiolytic yield of fluoride (G_{F^-}, in 10^{-7} mol J^{-1}) for the defluorination of PFBS (initial concentration: 0.2 mM) with e_{aq}^- in the presence of different concentrations of SO_3^{2-} solutions from 0 to 1 M (all experimental data are fitted linearly within 10% accuracy). (b) Defluorination rate of PFBS in aqueous solution and varying concentrations of SO_3^{2-} and sulfate at 30 kGy. (c) ^{19}F NMR spectra of PFBS (initial concentration: 0.2 mM) irradiated with different absorbed doses in 0.1 M SO_3^{2-}. (d) Number of defluorination of degradation intermediates by HPLC-MS in 0.1 M SO_3^{2-}. (e) E_{EO} values for the defluorination of PFBS in different SO_3^{2-} concentrations (initial concentration: 0.2 mM for PFBS; inset red dashed line: E_{EO} value in UV/ARP with SO_3^{2-} of pH = 12 from Liu et al.[11]).

defluorination. On the other hand, the continuous increase in SO_3^{2-} concentration resulted in aggregation and micellization. This is why a higher concentration than 0.2 M SO_3^{2-} would reduce the reactivity of PFBS with e_{aq}^- and yield negative effects. The combined influence of these two factors ultimately determined the PFBS reactivity at different SO_3^{2-} concentrations.

Accelerated PFBS Defluorination Activated by SO_3^{2-}. Perfluoroalkyl sulfonates (PFSAs) exhibit a higher resistance to photolytic e_{aq}^- treatment than perfluoroalkyl carboxylates (PFCA). Particularly, short-chain PFSA species pronounced notably sluggish reactivity toward e_{aq}^-. Achieving an effective defluorination process necessitates higher chemical dosage and energy consumption. Our previous research demonstrated that the defluorination rate of PFBS by e_{aq}^- through γ-ray irradiation was limited to a mere 4% under pH = 10 conditions.[13] To enhance defluorination efficacy, we initially assessed the pH effects as reported before[10] (Figure 4a). Nevertheless, no discernible positive effect appeared even in pH = 12 solutions. The robust chemical resistance under highly alkaline conditions bottlenecked PFBS defluorination.

Aligned with the accelerated transient kinetics, higher SO_3^{2-} concentrations exhibited a markedly contrasting effect on the defluorination kinetics. In radiation chemistry, the G value, which refers to the number of various chemical species formed as a function of deposited energy, is used to evaluate PFSA defluorination efficiency.[31,32] As depicted in Figure 4a, the yield of released F^- (G_{F^-}) without SO_3^{2-} was found to be 0.02 $\times$ 10^{-7} mol J^{-1}. The addition of 0.05 M SO_3^{2-} sharply raised the yield 6-fold to 0.12 $\times$ 10^{-7} mol J^{-1} (Figure 4a). It is worth noting that the change in pH is almost negligible after irradiation (pH 11.97). G_{F^-} further increased to 0.26 $\times$ 10^{-7} mol J^{-1} in the presence of 0.1 M SO_3^{2-}. However, with excessive 0.5 M SO_3^{2-}, G_{F^-} decreased to 0.18 $\times$ 10^{-7} mol J^{-1} and eventually reached a near-saturation point of 0.11 $\times$ 10^{-7} mol J^{-1} at 1 M SO_3^{2-} (Figure 4a). The defluorination rate as a function of the SO_3^{2-} concentration shows two distinct effects on the PFBS defluorination process with SO_3^{2-} (Figure 4b), in accordance with our transient experiments. The highest defluorination rates occurred at 0.1 and 0.2 M SO_3^{2-} solutions, which enhanced to 43.7 and 43%, respectively. These rates were nearly 15 times higher than those without SO_3^{2-}. However, a further increase in SO_3^{2-} to 0.5 M led to a reduction in the defluorination rate to 30.1%. This reduction coincided with the decrease of the rate constant from 2.8 $\times$ 10^8 M^{-1} s^{-1} (at 0.1 M SO_3^{2-}) to 3.6−5.6 $\times$ 10^7 M^{-1} s^{-1} (at 0.5 M SO_3^{2-}). One may question whether SO_4^{2-} could play a similar interacting role as that of SO_3^{2-}. To address this, we also performed the reference experiments in 0.1 and 0.5 M SO_4^{2-} solution under identical gamma irradiation conditions. The obtained G_{F^-} and defluorination rates from 0.1 and 0.5 M SO_4^{2-} systems demonstrated a comparable level to that without SO_3^{2-} (Figure 4a,b). These distinct results confirmed the unique interaction between SO_3^{2-} and PFBS rather than a salt effect. Instead, the salt effect was attributed to the negative impact on G_{F^-} in the 0.5 and 1 M SO_3^{2-} systems.

Additionally, ^{19}F NMR spectroscopy confirmed the formation of the defluorination product (Figure 4c). As the absorbed dose increased, a new resonance corresponding to the defluorination product was built up and gradually predominated in the NMR spectra. This signal exclusively appeared at −124.3 ppm for 10 kGy and subsequently shifted to −123.3 ppm for 30 kGy without any other resonance. The sole signal indicated the presence of only one type of F atom in the defluorination product, which can be F^- ions or hydrodefluorination products.[37,44] High-performance liquid chromatography−mass spectrometry (HPLC-MS) unveiled a pronounced acceleration in the defluorination process under 0.1 M SO_3^{2-} from analysis of degradation intermediates (Figure 4d). In the absence of SO_3^{2-}, only the hydrodefluorination product ($C_4F_8HSO_3^-$), involving the removal of a single F atom, was identified after 30 kGy irradiation. However, the introduction of 0.1 M SO_3^{2-} resulted in the detection of $C_4F_4H_5SO_3^-$, marked by removing five F atoms,

https://doi.org/10.1021/acs.est.4c01444
Environ. Sci. Technol. XXXX, XXX, XXX−XXX

even after only 10 kGy of irradiation. As the absorbed dose reached 30 kGy, intermediates with removing seven fluorine atoms were observed. These further defluorination products under 0.1 M SO_3^{2-} reflected that PFBS was effectively defluorinated with an accelerated mechanism.

To estimate the practicality of the radiolysis approach, we also evaluated the electrical energy per order (E_{EO}, calculation details in the Supporting Information) level to evaluate the physical energy efficiency of SO_3^{2-} systems. E_{EO} is defined as the energy consumed to reduce the concentration of contaminant by 1 order of magnitude in 1 m^3 of water (eq 1).[5] It has recently been employed as a metric for comparing energy efficiency among PFAS degradative technologies.

$$E_{EO} = \ln(10) \times P/(k \times V) \quad (1)$$

where P is the power of the electron accelerator equivalent to the cobalt source (kW), k is the first-order rate constant (h^{-1}), and V is the volume of the solution (m^3). We are concerned more with defluorination than just reducing the PFxS concentration, so here, k is the rate constant for F^- release. To obtain the electric energy consumption, the power of the ^{60}Co γ-rays source is estimated from the equivalent electron accelerator as eq 2.

$$P = \frac{\dot{D} \times \rho \times V}{\eta} \quad (2)$$

where $\dot{D}$ is the dose rate, 2.25 kGy/h (Gy: J/kg), ρ is the density of the solution, 1 kg/dm^3, V is the volume of solution, 4×10^{-3} dm^3, and η is the accelerator electrical efficiency, which is around 10−40%.[46−48] $P_{average} = 2.25 \times 10^3 \times 1 \times 4 \times 10^{-3}/0.25/3600 = 1 \times 10^{-5}$ kW.

As illustrated in Figure 4e, the E_{EO} level dropped from 2326 to 134 kW h m^{-3}, which equaled only 58% of the current record in the UV-ARP system for PFBS (230 kW h m^{-3}). This remarkably high energy efficiency suggested a promising route to a cost-competitive defluorination process for short-chain PFSA, even superior to UV-ARP.

Reaction Pathway. On the basis of the SO_3^{2-}-accelerated defluorination mechanism, our studies were extended to longer-chain PFSA, specifically perfluorooctanesulfonate (PFOS, $C_8F_{17}SO_3^-$). As depicted in Figure 5a, G_F^- and the defluorination rate as a function of SO_3^{2-} exhibited a relationship similar to that observed in PFBS. The highest defluorination rate was achieved at 0.2 M SO_3^{2-}, reaching 25.4% after only 1.6 kGy irradiation. When converted into the E_{EO} level, this corresponded to 14 kW h m^{-3} (Figure 5b), only 35% of the current UV-ARP system record for PFOS (40 kW h m^{-3}). This value underscored the applicability of SO_3^{2-}-accelerated methods to PFSA homologues during irradiation. With an extended irradiation period of 20 kGy, the maximum defluorination rate reached 72.7%. The corresponding G_F^- was calculated to be 1.1×10^{-7} mol J^{-1} (Figure 5c).

Remarkably, the observed G_F^- value in Figure 5a reached 5.3 $\times 10^{-7}$ mol J^{-1}, greatly surpassing the theoretical yield of e_{aq}^- (2.7×10^{-7} mol J^{-1}). The unusual G value established the existence of an additional defluorination pathway distinct from the aforementioned discussion. To investigate further, we examined the steady-state intermediates using HPLC-MS. In addition to the hydrodefluorination products ($C_8F_{17-x}H_xSO_3^-$), we also detected a series of perfluoroalkyl carboxylates (PFCAs) with shorter-chain lengths (C3−C7, $C_{3-7}F_{7-15}COO^-$) as a function of absorbed dose (Figure 5d). DFT calculations also suggested that the BDE of the C−S bond declined from 50.6 to 49.8 kcal mol^{-1} in the presence of SO_3^{2-}. LUMO of PFBS with SO_3^{2-} is located on the sulfonic acid group of the PFBS molecule (Figure S6). These results strongly suggested the occurrence of a desulfurization/decarboxylation−hydroxylation−elimination−hydrolysis (DHEH) pathway.[42,49]

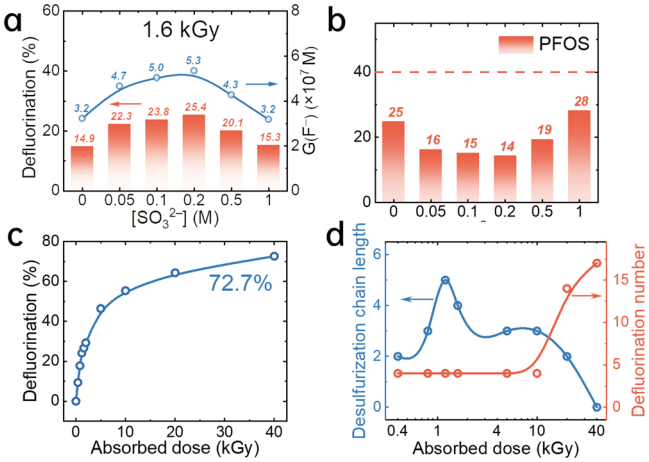

Figure 5. G_{F-} and the defluorination rate for the defluorination of PFOS with e_{aq}^- in different concentrations of SO_3^{2-} solutions at 1.6 kGy (a) and the corresponding E_{EO} values (b) (initial concentration: 0.2 mM for PFOS; inset red dashed line: E_{EO} value in UV/ARP with SO_3^{2-} of pH 12 from Liu et al.). (c) Defluorination rate of PFOS at an elevated absorbed dose to 40 kGy. (d) Number of desulfurization chain lengths and defluorination of degradation intermediates by HPLC-MS in 0.1 M SO_3^{2-}.

As proposed in the literature, when PFSA reacts with e_{aq}^- to form radical anions, it follows two distinct pathways.[50,51] First, sequential H/F exchanges take place and form highly recalcitrant hydrodefluorination products. Second, radical anions break the C−S bond between the headgroup and the perfluoroalkyl chain, yielding unstable perfluorinated alcohol (C_nF_{2n+1}−OH) that is prone to HF elimination. This acyl fluoride is hydrolyzed to release the second fluoride ion. The shorter-chain PFCA compounds initiate the next DHEH reaction cycle. Essentially, during one DHEH reaction cycle, the consumption of one e_{aq}^- can realize the removal of two F atoms.

As shown in Figure S7, in the absence of SO_3^{2-}, hydrodefluorination products from the defluorination process were restricted to four H/F exchange steps. This limitation is attributed to the formation of the highly recalcitrant $C_8F_{13}H_4SO_3^-$ product. Moreover, the DHEH pathway without SO_3^{2-} was constrained to 3 cycles and produced the $C_5F_{11}COO^-$ product. In comparison, the introduction of 0.1 M SO_3^{2-} achieved seven DHEH cycles and the formation of the all-site H/F exchange product ($C_8H_{17}SO_3^-$). Such a new reaction pathway transcended the limitation of defluorination in the absence of SO_3^{2-}. As shown in Figure 5d, 0.1 M SO_3^{2-} facilitated the initial DHEH reaction, even at a low dose of 0.4 kGy. Five cycles of DHEH were observed and generated a $C_3F_7COO^-$ product at 1.2 kGy. Beyond this point, no further DHEH reactions occurred. Continuous irradiation resulted in the gradual degradation of the PFCA products obtained from DHEH until 40 kGy, corresponding to the descent of the shortened chain length curve after 1.2 kGy. Regarding the defluorination process, the number of defluorination was

https://doi.org/10.1021/acs.est.4c01444
Environ. Sci. Technol. XXXX, XXX, XXX−XXX

suppressed to four up to 10 kGy. This can be attributed to the persistence of the $C_8F_{13}H_4SO_3^-$ compound and favored e_{aq}^- toward predominately the DHEH reaction pathway. After surpassing 10 kGy, defluorination of $C_8F_{13}H_4SO_3^-$ was also induced in the presence of 0.1 M SO_3^{2-}, ultimately realizing all-site defluorination.

More importantly, we can quantify the fraction of $PFOS^{\cdot-}$ radical anions that engage in distinct pathways (DHEH or H/F exchange) by referencing the G_F^- value in Figure 5a. The Ge_{aq}^- is known to be 2.7×10^{-7} mol J^{-1} in the absence of SO_3^{2-}. By examining the observed G_F^- value of 3.2×10^{-7} mol J^{-1}, it became evident that approximately 82% of $PFOS^{\cdot-}$ radicals underwent H/F exchanges, while the remaining 18% of $PFOS^{\cdot-}$ radicals followed the DHEH pathway. Conversely, as the concentration of SO_3^{2-} ranging from 0.05 to 0.2 M, the proportion of $PFOS^{\cdot-}$ radicals participating in the DHEH reaction raised from 74% up to 96%. This increase corresponds to the elevated G_F^- value reaching as high as 5.3×10^{-7} mol J^{-1}. These findings unveil that the presence of SO_3^{2-} not only activates the C−F bonds but also influences the C−S bond of PFOS. During the degradation of PFOS by e_{aq}^- in the presence of SO_3^{2-}, e_{aq}^- initially reacts with PFOS to form radical anions $PFOS^{\cdot-}$ (e_{aq}^- + PFOS → $PFOS^{\cdot-}$). Under SO_3^{2-}-assisted activation of the C−S bond, $PFOS^{\cdot-}$ first predominately follows the DHEH reaction pathway to generate shorter-chain PFCA intermediates. The DHEH reaction achieves effective defluorination rather than H/F exchange. After sufficient DHEH reactions, $PFOS^{\cdot-}$ next enters the H/F defluorination process. According to the previous report,[52] the theoretical calculation elucidated that the sulfonic functional group in PFOS caused the C_3 and C_4 centers to have the lowest bond dissociation energy among all the C−F bonds. e_{aq}^- preferentially attacks either the C_3 or C_4 sites at the center of the molecule. With the weakened C−F bonds activated by SO_3^{2-}, e_{aq}^- could continue H/F exchange until all F atoms are removed.

■ ASSOCIATED CONTENT

Supporting Information

The Supporting Information is available free of charge at https://pubs.acs.org/doi/10.1021/acs.est.4c01444.

Transient absorption kinetic of $SO_3^{\cdot-}$ radicals and of e_{aq}^- in the absence of SO_3^{2-}. HPLC-MS results in the presence of 0.1 M tert-butanol without SO_3^{2-} (PDF)

■ AUTHOR INFORMATION

Corresponding Authors

Mehran Mostafavi − *Institute de Chimie Physique, UMR8000 CNRS/Université Paris-Saclay, Orsay 91405, France;* orcid.org/0000-0002-4510-8272; Email: mehran.mostafavi@universite-paris-saclay.fr

Jun Ma − *School of Nuclear Science and Technology, University of Science and Technology of China, Hefei, Anhui 230026, China;* orcid.org/0000-0001-7776-0751; Email: majun0502@ustc.edu.cn

Authors

Zhiwen Jiang − *School of Nuclear Science and Technology, University of Science and Technology of China, Hefei, Anhui 230026, China; Institute de Chimie Physique, UMR8000 CNRS/Université Paris-Saclay, Orsay 91405, France;* orcid.org/0000-0003-3576-2534

Sergey Denisov − *Institute de Chimie Physique, UMR8000 CNRS/Université Paris-Saclay, Orsay 91405, France;* orcid.org/0000-0001-7881-1979

Daniel Adjei − *Institute de Chimie Physique, UMR8000 CNRS/Université Paris-Saclay, Orsay 91405, France*

Complete contact information is available at: https://pubs.acs.org/10.1021/acs.est.4c01444

Author Contributions

Z.W.J., J.M., and M.M. conceived of the work; Z.W.J., D.A., and S.A.D. designed and performed the experiments; Z.W.J., D.A., J.M., and M.M. analyzed the data; Z.W.J. and M.M. wrote the manuscript; J.M. and M.M. deeply revised the manuscript.

Funding

This work was supported by the National Natural Science Foundation of China (11975122), Jiangsu Province Science Fund for Distinguished Young Scholars (BK20230032), Fundamental Research Funds for the Central Universities (NE2020006), Scientific and Technological Innovation Special Fund for Carbon Peak and Carbon Neutrality of Jiangsu Province (BK20220026), and Postdoctoral Fellowship Program of CPSF (GZC20232529).

Notes

The authors declare no competing financial interest.

■ ACKNOWLEDGMENTS

We thank Jean-Philippe Larbre for his help during the experiments at ELYSE. Guillaume Van Der Rest and Estelle Loire are gratefully acknowledged for their assistance in the HPLC-MS experiments. We also acknowledge Jean-Pierre Baltaze for the NMR experiments.

■ REFERENCES

(1) Panieri, E.; Baralic, K.; Djukic-cosic, D.; Djordjevic, A. B.; Saso, L. PFAS Molecules: A Major Concern for the Human Health and the Environment. *Toxics* **2022**, *10* (2), 44.

(2) Wang, J.; Lin, Z.; He, X.; Song, M.; Westerhoff, P.; Doudrick, K.; Hanigan, D. Critical Review of Thermal Decomposition of Per- and Polyfluoroalkyl Substances: Mechanisms and Implications for Thermal Treatment Processes. *Environ. Sci. Technol.* **2022**, *56* (9), 5355−5370.

(3) Bao, Y.; Deng, S.; Jiang, X.; Qu, Y.; He, Y.; Liu, L.; Chai, Q.; Mumtaz, M.; Huang, J.; Cagnetta, G.; Yu, G. Degradation of PFOA Substitute: GenX (HFPO-DA Ammonium Salt): Oxidation with UV/Persulfate or Reduction with UV/Sulfite? *Environ. Sci. Technol.* **2018**, *52* (20), 11728−11734.

(4) Cui, J.; Gao, P.; Deng, Y. Destruction of Per- and Polyfluoroalkyl Substances (PFAS) with Advanced Reduction Processes (ARPs): A Critical Review. *Environ. Sci. Technol.* **2020**, *54* (7), 3752−3766.

(5) Fennell, B. D.; Mezyk, S. P.; Mckay, G. Critical Review of UV-Advanced Reduction Processes for the Treatment of Chemical Contaminants in Water. *ACS Environ. Au* **2022**, *2* (3), 178−205.

(6) Banayan esfahani, E.; Asadi zeidabadi, F.; Zhang, S.; Mohseni, M. Photo-Chemical/Catalytic Oxidative/Reductive Decomposition of per- and Poly-Fluoroalkyl Substances (PFAS), Decomposition Mechanisms and Effects of Key Factors: A Review. *Environ. Sci. Water Res.* **2022**, *8* (4), 698−728.

(7) Liu, Z.; Bentel, M. J.; Yu, Y.; Ren, C.; Gao, J.; Pulikkal, V. F.; Sun, M.; Men, Y.; Liu, J. Near-Quantitative Defluorination of Perfluorinated and Fluorotelomer Carboxylates and Sulfonates with Integrated Oxidation and Reduction. *Environ. Sci. Technol.* **2021**, *55* (10), 7052−7062.

(8) Gao, J.; Liu, Z.; Bentel, M. J.; Yu, Y.; Men, Y.; Liu, J. Defluorination of Omega-Hydroperfluorocarboxylates (ω-HPFCAs):

Distinct Reactivities from Perfluoro and Fluorotelomeric Carboxylates. *Environ. Sci. Technol.* **2021**, *55* (20), 14146−14155.
(9) Song, Z.; Tang, H.; Wang, N.; Zhu, L. Reductive Defluorination of Perfluorooctanoic Acid by Hydrated Electrons in a Sulfite-Mediated UV Photochemical System. *J. Hazard. Mater.* **2013**, *262*, 332−338.
(10) Bentel, M. J.; Liu, Z.; Yu, Y.; Gao, J.; Men, Y.; Liu, J. Enhanced Degradation of Perfluorocarboxylic Acids (PFCAs) by UV/Sulfite Treatment: Reaction Mechanisms and System Efficiencies at pH 12. *Environ. Sci. Technol. Lett.* **2020**, *7* (5), 351−357.
(11) Liu, Z.; Chen, Z.; Gao, J.; Yu, Y.; Men, Y.; Gu, C.; Liu, J. Accelerated Degradation of Perfluorosulfonates and Perfluorocarboxylates by UV/Sulfite + Iodide: Reaction Mechanisms and System Efficiencies. *Environ. Sci. Technol.* **2022**, *56* (6), 3699−3709.
(12) Hou, C.; Deng, J.; Li, S.; Li, H.; Zhou, Y.; Zhai, Y. Differences between Reductive Defluorination of Perfluorooctanoic Acid by Chlorination, Bromination, and Iodization in the Vacuum-Ultraviolet/Sulfite Process. *J. Hazard. Mater.* **2023**, *460*, No. 132459.
(13) Gu, Y.; Liu, T.; Wang, H.; Han, H.; Dong, W. Hydrated Electron Based Decomposition of Perfluorooctane Sulfonate (PFOS) in the VUV/Sulfite System. *Sci. Total Environ.* **2017**, *607*, 541−548.
(14) Gu, Y.; Dong, W.; Luo, C.; Liu, T. Efficient Reductive Decomposition of Perfluorooctanesulfonate in a High Photon Flux UV/Sulfite System. *Environ. Sci. Technol.* **2016**, *50* (19), 10554−10561.
(15) Qu, Y.; Zhang, C.; Li, F.; Chen, J.; Zhou, Q. Photo-Reductive Defluorination of Perfluorooctanoic Acid in Water. *Water Res.* **2010**, *44* (9), 2939−2947.
(16) Park, H.; Vecitis, C. D.; Cheng, J.; Choi, W.; Mader, B. T.; Hoffmann, M. R. Reductive Defluorination of Aqueous Perfluorinated Alkyl Surfactants: Effects of Ionic Headgroup and Chain Length. *J. Phys. Chem. A* **2009**, *113* (4), 690−696.
(17) Jiang, Z.; Adjei, D.; Denisov, S. A.; Mostafavi, M.; Ma, J. Transient Kinetics of Short-Chain Perfluoroalkyl Sulfonate with Radiolytic Reducing Species. *Environ. Sci. Technol. Lett.* **2023**, *10* (1), 59−65.
(18) Van hoomissen, D. J.; Vyas, S. Early Events in the Reductive Dehalogenation of Linear Perfluoroalkyl Substances. *Environ. Sci. Technol. Lett.* **2019**, *6* (6), 365−371.
(19) Liu, G.; Feng, C.; Shao, P. Degradation of Perfluorooctanoic Acid with Hydrated Electron by a Heterogeneous Catalytic System. *Environ. Sci. Technol.* **2022**, *56* (10), 6223−6231.
(20) Maza, W. A.; Breslin, V. M.; Feygelson, T. I.; Desario, P. A.; Pate, B. B.; Owrutsky, J. C.; Epshteyn, A. Degradation of Perfluorooctanesulfonate (PFOS) by Sub-Bandgap Irradiation of Hydrogen-Terminated Nanodiamond. *Appl. Catal., B* **2023**, *325*, No. 122306.
(21) Dong, Z.; Wang, Y.; Wen, D.; Peng, J.; Zhao, L.; Zhai, M. Recent Progress in Environmental Applications of Functional Adsorbent Prepared by Radiation Techniques: A Review. *J. Hazard. Mater.* **2022**, *424*, No. 126887.
(22) Abou taleb, M. F.; Abou el fadl, F. I.; Albalwi, H. Adsorption of Toxic Dye in Wastewater onto Magnetic NVP/CS Nanocomposite Hydrogels Synthesized Using Gamma Radiation. *Sep. Purif. Technol.* **2021**, *266*, No. 118551.
(23) Hina, H.; Nafees, M.; Ahmad, T. Treatment of Industrial Wastewater with Gamma Irradiation for Removal of Organic Load in Terms of Biological and Chemical Oxygen Demand. *Heliyon* **2021**, *7* (2), No. e05972.
(24) Wang, J.; Chu, L. Irradiation Treatment of Pharmaceutical and Personal Care Products (PPCPs) in Water and Wastewater: An Overview. *Radiat. Phys. Chem.* **2016**, *125*, 56−64.
(25) Wang, J.; Zhuan, R.; Chu, L. The Occurrence, Distribution and Degradation of Antibiotics by Ionizing Radiation: An Overview. *Sci. Total Environ.* **2019**, *646*, 1385−1397.
(26) Cho, J. Y.; Chung, B. Y.; Lee, K. B.; Lee, G. H.; Hwang, S. A. Decomposition Reaction of the Veterinary Antibiotic Ciprofloxacin Using Electron Ionizing Energy. *Chemosphere* **2014**, *117* (1), 158−163.
(27) Michael, I.; Rizzo, L.; Mcardell, C. S.; Manaia, C. M.; Merlin, C.; Schwartz, T.; Dagot, C.; Fatta-kassinos, D. Urban Wastewater Treatment Plants as Hotspots for the Release of Antibiotics in the Environment: A Review. *Water Res.* **2013**, *47* (3), 957−995.
(28) Amador, C. K.; Cavalli, H.; Tenorio, R.; Tetu, H.; Higgins, C. P.; Vyas, S.; Strathmann, T. J. Influence of Carbonate Speciation on Hydrated Electron Treatment Processes. *Environ. Sci. Technol.* **2023**, *57* (20), 7849−7857.
(29) Belloni, J.; Monard, H.; Gobert, F.; Larbre, J. P.; Demarque, A.; De waele, V.; Lampre, I.; Marignier, J. L.; Mostafavi, M.; Bourdon, J. C.; Bernard, M.; Borie, H.; Garvey, T.; Jacquemard, B.; Leblond, B.; Lepercq, P.; Omeich, M.; Roch, M.; Rodier, J.; Roux, R. ELYSE-A picosecond electron accelerator for pulse radiolysis. *Instr. Meth. Phys. Res. A* **2005**, *539* (3), 527−539.
(30) Marignier, J. L.; De waele, V.; Monard, H.; Gobert, F.; Larbre, J. P.; Demarque, A.; Mostafavi, M.; Belloni, J. Time-resolved spectroscopy at the picosecond laser-triggered electron accelerator ELYSE. *Radiat. Phys. Chem.* **2006**, *75* (9), 1024−1033.
(31) Bentel, M. J.; Yu, Y.; Xu, L.; Kwon, H.; Li, Z.; Wong, B. M.; Men, Y.; Liu, J. Degradation of Perfluoroalkyl Ether Carboxylic Acids with Hydrated Electrons: Structure-Reactivity Relationships and Environmental Implications. *Environ. Sci. Technol.* **2020**, *54* (4), 2489−2499.
(32) Banerjee, B.; Paria, S. Effect of Electrolytes on Solution and Interfacial Behaviors of Double Chain Cationic-Nonionic Surfactant Mixtures for Hydrophobic Surface Wetting and Oil/Water Emulsion Stability Applications. *Langmuir* **2021**, *37* (35), 10560−10572.
(33) Qazi, M. J.; Schlegel, S. J.; Backus, E. H. G.; Bonn, M.; Bonn, D.; Shahidzadeh, N. Dynamic Surface Tension of Surfactants in the Presence of High Salt Concentrations. *Langmuir* **2020**, *36* (27), 7956−7964.
(34) Hayon, E.; Treinin, A.; Wilf, J. Electronic Spectra, Photochemistry, and Autoxidation Mechanism of the Sulfite-Bisulfite-Pyrosulfite Systems. SO_2^-, SO_3^-, SO_4^-, and SO_5^- Radicals. *J. Am. Chem. Soc.* **1972**, *94* (1), 47−57.
(35) Huie, R. E.; Clifton, C. L.; Altstein, N. A Pulse Radiolysis and Flash Photolysis Study of the Radicals SO_2^-, SO_3^-, SO_4^- and SO_5^-. *Int. J. Radiat. Appl. Instrum. C. Radiat. Phys. Chem.* **1989**, *33* (4), 361−370.
(36) Ellis, D. A.; Denkenberger, K. A.; Burrow, T. E.; Mabury, S. A. The Use of ^{19}F NMR to Interpret the Structural Properties of Perfluorocarboxylate Acids: A Possible Correlation with Their Environmental Disposition. *J. Phys. Chem. A* **2004**, *108* (46), 10099−10106.
(37) Heerah, K.; Waclawek, S.; Konzuk, J.; Longstaffe, J. G. Benchtop ^{19}F NMR Spectroscopy as a Practical Tool for Testing of Remedial Technologies for the Degradation of Perfluorooctanoic Acid, a Persistent Organic Pollutant. *Magn. Reson. Chem.* **2020**, *58* (12), 1160−1167.
(38) Li, H.; Wang, X.; Zhong, J.; Chu, B.; Ma, Q.; Zeng, X. C.; Francisco, J. S.; He, H. Mechanistic Study of the Aqueous Reaction of Organic Peroxides with HSO_3^- on the Surface of a Water Droplet. *Angew. Chem., Int. Ed.* **2021**, *60* (37), 20200−20203.
(39) Ning, C.; Ma, H.; Pedersen, C. M.; Chang, H.; Wang, Y.; Qiao, Y. Interaction between Environmental Contaminant PFOA and PAMAM in Water: ^{19}F and ^{1}H NMR Studies. *J. Mol. Liq.* **2019**, *283*, 45−50.
(40) Arsenault, G.; Chittim, B.; Gu, J.; Mcalees, A.; Mccrindle, R.; Robertson, V. Separation and Fluorine Nuclear Magnetic Resonance Spectroscopic (^{19}F NMR) Analysis of Individual Branched Isomers Present in Technical Perfluorooctanesulfonic Acid (PFOS). *Chemosphere* **2008**, *73* (1), S53−S59.
(41) Wang, X.; Chen, J.; Wang, D.; Dong, S.; Hao, J.; Hoffmann, H. Monitoring the Different Micelle Species and the Slow Kinetics of Tetraethylammonium Perfluorooctane-Sulfonate by ^{19}F NMR Spectroscopy. *Adv. Colloid Interface Sci.* **2017**, *246*, 153−164.
(42) Bentel, M. J.; Yu, Y.; Xu, L.; Li, Z.; Wong, B. M.; Men, Y.; Liu, J. Defluorination of Per- and Polyfluoroalkyl Substances (PFASs) with Hydrated Electrons: Structural Dependence and Implications to

https://doi.org/10.1021/acs.est.4c01444
Environ. Sci. Technol. XXXX, XXX, XXX−XXX

PFAS Remediation and Management. *Environ. Sci. Technol.* **2019**, *53* (7), 3718−3728.
(43) Chen, Z.; Li, C.; Gao, J.; Dong, H.; Chen, Y.; Wu, B.; Gu, C. Efficient Reductive Destruction of Perfluoroalkyl Substances under Self-Assembled Micelle Confinement. *Environ. Sci. Technol.* **2020**, *54* (8), 5178−5185.
(44) Rafique, A. S.; Khodaparast, S.; Poulos, A. S.; Sharratt, W. N.; Robles, E. S. J.; Cabral, J. T. Micellar Structure and Transformations in Sodium Alkylbenzenesulfonate (NaLAS) Aqueous Solutions: Effects of Concentration, Temperature, and Salt. *Soft Matter* **2020**, *16* (33), 7835−7844.
(45) Borisov, O. V.; Zhulina, E. B. Effect of Salt on Self-Assembly in Charged Block Copolymer Micelles. *Macromolecules* **2002**, *35* (11), 4472−4480.
(46) Sun, J.; Jennepalli, S.; Lee, M.; O'carroll, D. M.; Åkermark, B.; Manefield, M. J.; Das, B.; Kumar, N. Removal of Per- And Polyfluoroalkyl Substances (PFAS) from Water by Ceric (IV) Ammonium Nitrate. *RSC Adv.* **2021**, *11* (29), 17642−17645.
(47) Chmielewski, A. G.; Al-sheikhly, M.; Berejka, A. J.; Cleland, M. R.; Antoniak, M. Recent Developments in the Application of Electron Accelerators for Polymer Processing. *Radiat. Phys. Chem.* **2014**, *94* (1), 147−150.
(48) Zimek, Z. Impact of Electron Accelerator Technical and Economic Parameters on Unit Cost of Radiation Processing. *Radiat. Phys. Chem.* **2021**, *189*, No. 109713.
(49) Amador, C. K.; Van hoomissen, D. J.; Liu, J.; Strathmann, T. J.; Vyas, S. Ultra-Short Chain Fluorocarboxylates Exhibit Wide Ranging Reactivity with Hydrated Electrons. *Chemosphere* **2023**, *311* (1), No. 136918.
(50) Trojanowicz, M.; Bojanowska-czajka, A.; Bartosiewicz, I.; Kulisa, K. Advanced Oxidation/Reduction Processes Treatment for Aqueous Perfluorooctanoate (PFOA) and Perfluorooctanesulfonate (PFOS) − A Review of Recent Advances. *Chem. Eng. J.* **2018**, *336*, 170−199.
(51) Trang, B.; Li, Y.; Xue, X. S.; Ateia, M.; Houk, K. N.; Dichtel, W. R. Low-Temperature Mineralization of Perfluorocarboxylic Acids. *Science* **2022**, *377* (6608), 839−845.
(52) Biswas, S.; Yamijala, S. S.; Wong, B. M. Degradation of per-and polyfluoroalkyl substances with hydrated electrons: a new mechanism from first-principles calculations. *Environ. Sci. Technol.* **2022**, *56* (12), 8167−8175.

https://doi.org/10.1021/acs.est.4c01444
Environ. Sci. Technol. XXXX, XXX, XXX−XXX